Carbohydrate Polymers 84 (2011) 975–983

Contents lists available at ScienceDirect

Carbohydrate Polymers

journal homepage: www.elsevier.com/locate/carbpol

Nanofibrillated cellulose from TEMPO-oxidized eucalyptus fibres: Effect of the carboxyl content

Iskander Besbes, Sabrine Alila, Sami Boufi*

LMSE, Faculté des Sciences de Sfax, University of Sfax, BP 802-3018 Sfax, Tunisia

ARTICLE INFO

Article history:
Received 6 November 2010
Received in revised form 9 December 2010
Accepted 16 December 2010
Available online 23 December 2010

Keywords:
Nanofibrillated cellulose
Cellulose
Eucalyptus
Nanocomposite

ABSTRACT

In the present work the effect of the carboxyl content on the high pressure defibrillation of oxidized eucalyptus from micro to nanoscale size was investigated. It has been shown that TEMPO-mediated oxidation of dried softwood pulp not only facilitates the defibrillation process, but also reduces the number of passes necessary to get the gel, as well as preventing the clogging of the homogenizer. In fact, these effects became apparent up to a carboxyl content about 300 μmol/g, and over 500 μmol/g, the yield in the nanofibrillated cellulose exceeded 90%, at a defibrillation pressure of 600 bar. The morphology of the ensuing nanofibrillated cellulose (NFC) and its crystalline degree were characterised by FE-SEM and DRX measurement, respectively. The evolution of the transparency degree and the viscosity according to the oxidation degree and defibrillation pressure were also analysed by UV–vis transmittance and rheological measurement.

The reinforcing potential of the ensuing NFC was explored by means of dynamic mechanical analysis (DMA) carried on nanocomposite film prepared from a suspension of NFC as the reinforcing phase and an acrylic latex dispersion as the matrix.

1. Introduction

It goes without saying that lignocellulosic fibres as reinforcing elements in polymeric matrices are considered as one of the most promising fillers in for sustainable composite materials. Unlike the conventional engineering fibres, e.g. glass and carbon fibres, lignocellulosic fibres provide many advantages that are well reported in numerous reviews (Bledzki & Gassan, 1999; Jacob & Thomas, 2008; Mohanty, Misra, & Drzal, 2001). Among them, one can cite the low density, the low cost, the renewable character, the non-abrasive properties, the high specific strength and the safer handling compared with synthetic reinforcements. However, despite the high specific tensile strength and tensile modulus of cellulose fibres, their reinforcing potential remains modest for different reasons. First of all, the presence of defects along the fibre axes results in a local stress concentration leading to a premature breaking. Secondly, the hydrophilic character of natural fibres adversely affects adhesion to a hydrophobic matrix, thus resulting in a poor strengthening effect. Eventually, the limited aspect ratio of the fibres is likely to undergo notable drop after processing involving shearing.

For a better exploitation of reinforcing potential of individual fibres, one can call on the nano-sized cellulosic material as reinforcement instead of micro-sized fibres to prepare nanocomposite with high strength, stiffness, and transparency. Among the nano-sized reinforcements, nanofibrillated cellulose (often called also microfibrillated cellulose (MFC)) is one of the most promising natural nanofillers (Siro & Plackett, 2010). Indeed, for rod-like nanofiller the reinforcing potential is controlled by the aptitude of the nanofiller to form a percolated network. In the particular case of cellulose-based nanofillers, a strong rigid percolating nanofiller network held through strong hydrogen bonding interactions contribute to boost the modulus as well as the strengthening potential of the nanofiller (Azizi Samir, Alloin, Paillet, & Dufresne, 2004; Malainine, Mahrouz, & Dufresne, 2005a).

The nanofibrillated material consists of interconnected fibrils and microfibrils, whose width is 10–100 nm and length varies from 100 nm to several micrometers depending on the source of cellulose. The nanofibrillated cellulose derived from wood was first reported by Turbak et al. more than two decades ago (Herrick, Casebier, Hamilton, & Sandberg, 1983; Turbak, Snyder, & Sandberg, 1983). It was obtained through a mechanical treatment of pulp fibres, consisting of refining and high pressure homogenizing processes, thus giving rise to a gel-like, highly viscous dispersion at relatively low concentrations, i.e. 2% aqueous suspension. Thanks to their structure with an arrangement of crystallite strands packed in a dense association of cellulose molecules (between 20 and 60 chains) aligned more or less with the fibre axis, the lack of chain folding with only a small number of defects, the exceptional mechanical properties, including a high Young's modulus (138 GPa in the crystal region along the longitudinal direction)

* Corresponding author.
E-mail address: sami.boufi@fss.rnu.tn (S. Boufi).

0144-8617/$ – see front matter © 2010 Elsevier Ltd. All rights reserved.
doi:10.1016/j.carbpol.2010.12.052

(Nishino, Takano, & Nakamae, 1995), a high strength and a very low coefficient of thermal expansion, the nano-sized cellulose filler offer great potential for use as reinforcement in nanocomposites (Bendahou, Kaddami, & Dufresne, 2010; Johnson, Zink-Sharp, Renneckar, & Glasser, 2009; Iwamoto, Nakagaito, Yano, & Nogi, 2005).

Despite the high potential of NFC, it was not until 2000 that NFC stirred up much interest. The most adopted method of preparing NFC consists of submitting a dilute fibre suspension with a concentration lower than 1–2 wt.% through a mechanical homogenizer in which a large pressure drop facilitates microfibrillation (Malainine, Mahrouz, & Dufresne, 2005b; Nakagaito & Yano, 2004). When a cellulosic pulp fibre suspension is homogenized, the procedure is often repeated through several passes in order to increase the degree of fibrillation (Jacob & Thomas, 2008; Mohanty et al., 2001; Siro & Plackett, 2010). A higher number of passes obviously increases the energy required for disintegration. In order to facilitate disintegration and lower the energy input, one may reduce the fibre's length by mechanical cutting (Leitner, Hinterstoisser, Wastyn, Keckes, & Gindl, 2007), cryocrushing (Alemdar & Sain, 2008), ultrasonic (Johnson et al., 2009) or chemical treatments such as acid hydrolysis prior to mechanical treatments prior to homogenization (Boldizar, Klason, Kubat, Naslund, & Saha, 1987). Enzyme treatment was also found to facilitate disintegration, and the nanofibrillated nanofibers produced go through lower degradation effect (Henriksson, Henriksson, Berglund, & Lindstrom, 2007; Pääkkö et al., 2007). More recently, a single-pass grinder treatment of never-dried pulp submitted to extraction to remove lignin and hemicellulose has been proven to be effective to obtain 10–20 nm wide cellulose nanofibres (Abe, Iwamoto, & Yano, 2007; Iwamoto, Abe, & Yano, 2008).

Another promising route towards making the preparation of the suspensions of individual NFC easier relies on chemical treatments involving the addition of negatively charged entities at the microfibrils surface. These charges and their repulsive effect greatly enhance the ease of separation of individual microfibrils. These approaches were introduced by Saito et al. (Saito et al., 2009; Saito & Isogai, 2004; Saito, Kimura, Nishiyama, & Isogai, 2007; Saito, Nishiyama, Putaux, Vignon, & Isogai, 2006) and Wågberg et al. (2008). Wågberg et al. reported a chemical pre-treatment procedure in which delignified softwood pulp fibres were carboxymethylated prior to disintegration in a high-pressure fluidizer. Saito et al. presented an oxidation pre-treatment method for hardwood pulp fibres using 2,2,6,6,-tetramethylpiperidine-1-oxyl radical (TEMPO)-mediated system followed by very mild mechanical disintegration (Saito et al., 2007). However, such procedures were efficient only for never-dried fibres and the yield in MCF was within 40–70%.

The aim of the present study is to clarify the effect of the oxidation treatment and extent of bleached deliginified cellulose fibres already dried on the number of passes necessary to bring on the fibre's fibrillation using homogenizing treatment. The reinforcing potential of the ensuing microfibrillated cellulose was investigated by preparing nanocomposite film and analyzing the mechanical properties using DMA and long range deformation. Besides, the structural details of the NFC were studied with SEM, and the crystallinity was determined before and after different stages of the homogenization process using DRX and Raman spectroscopy.

2. Experimental

2.1. Materials

Commercial bleached eucalyptus pulp (*Eucalyptus globulus*) was used as starting material for the preparation of NFC. The other chemical products were purchased from Sigma Aldrich and used without purification.

2.2. TEMPO-mediated oxidation

Cellulose fibres (5 g) were dispersed in 0.05 M sodium phosphate buffer (500 mL, pH 7) containing TEMPO (25 mg) and NaBr (250 mg). Sodium chlorite (80%, 1.13 g, 10 mmol) and the 2 M sodium hypochlorite solution (0.5 mL, 1.0 mmol) were added in one step to the flask. The latter was well-sealed and stirred at 500 rpm and 60 °C for a designated time (2–72 h). During the oxidation process, the colour turned yellow as a result of the generation of free chlorine. The oxidation was stopped by adding 100 mL of ethanol, and oxidized fibres were filtered and washed twice with deionised water. After cooling the suspension to room temperature, the oxidized cellulose fibres were completely washed with water by filtration.

2.3. Carboxyl content

The carboxylate contents of the oxidized cellulose were determined using conductometric titration. The wet fibres (50–100 mg) were suspended in 15 mL of a 0.01 M HCl solution to exchange the sodium cations bound to the carboxyl groups by hydrogen ions. When a stable suspension was obtained, the mixture was titrated with 0.01 M NaOH. The titration curves showed the presence of a strong acid corresponding to the excess of HCl and a weak acid corresponding to the carboxylate content, the total amount of carboxyl groups was calculated from:

$$C = (V_1 - V_0) \times C_{NaOH}$$

with C, the carboxyl content; V_1 and V_0, the equivalent volumes of added NaOH solution; C_{NaOH}, the exact concentration of NaOH solution; m, the weight of dried product.

In the following the oxidized samples are identified as *Eucal-X*, where X represents the carboxyl content.

2.4. Fibres morphology

The fibre's morphology was determined using MorFI (LB-01) analyser. The technique is based on the image analysis of a diluted fibres suspension with a CCD video-camera.

2.5. Preparation of microfibrils

The fibre suspension was dispersed in water at a fibre content of 1–2 wt.% and then homogenized by different passes through a high pressure homogenizer (NS1001L PANDA 2K-GEA) operating at pressure ranging from 100 to 1000 bar and at a temperature operating between 60 and 70 °C until obtaining a translucent gel. Unless specified, the pH of the fibre suspension was neutral.

2.6. Yield in NFC

A diluted gel (0.2% solid content) was centrifuged at 4500 rpm for 20 min to separate the nanofibrillated material (in supernatant fraction) from non-fibrillated and partially fibrillated fibres which sediment. The sediment fraction was dried to constant weight at 90 °C in a halogen desiccator and the yield of the nanofibrillated fraction was calculated from:

$$\text{Yield}\,\% = \left(1 - \frac{\text{weight of dried sediment}}{(\text{weight of diluted sample} \times \ \%\text{Sc})}\right) \times 100$$

%Sc = solid content of the diluted gel sample.

The results represent the averages of three replicates.

2.7. Nanocomposites processing

A commercial latex obtained by the copolymerization of styrene (34 wt.%) and butyl acrylate (64 wt.%), and containing 1 wt.% acrylic acid and 1 wt.% acrylamide, and provided by MPC-Prokim (Tunisia) was used as a polymer matrix. The average particle size of the polymer dispersion is around 140 nm, and the glass–rubber transition temperature (T_g) of the poly(S-co-BuA) copolymer was around 25 °C. the nanocomposite film was prepared by mixing the NFC suspensions (solid fraction 1–2 wt.%) in a various proportion with the polymer dispersion. After the mixing was complete, this mixture was poured into a in a Teflon mould and allowed to dry under ambient condition for two days, followed by a post storing at 50 °C for 3 h to achieve complete drying and coalescence of polymer particles. The nanocomposite film obtained was translucent to transparent, according to the NFC content with a thickness in the range of 300–400 μm.

2.8. X-ray diffraction analysis

The crystalline degree of cellulose was calculated from an X-ray diffraction profile. X-ray measurements were made on sample sheets cut in small pieces after the air drying of the nanofibres suspension. Cu Kα radiation, generated with a Bruker AXS diffractometer (Bruker AXS, Madison, WI at 30 kV, 100 mA. Sweeps of 5–50° 2θ were made with a step size of 0.05 s and step time measurement of 10 s. The crystalline index (CrI) was calculated using the diffraction intensities of the crystalline structure and that of the amorphous fraction according to the method of Segal, Creely, Martin and Conrad (1959):

$$\mathrm{CrI\%} = \left[\frac{I_{002} - I_{\mathrm{am}}}{I_{002}}\right] \times 100$$

where I_{002} is the intensity of the crystalline peak at the maximum at 2θ between 22° and 23° for cellulose *I*, and I_{am} is the intensity at the minimum at 2θ between 18° and 19° for cellulose *I*.

2.9. Rheological measurements

Rheological measurements were carried out using a controlled speed rotating rheometer (Rheotec RS-30) operated with cone-and-plate geometries (cone angle: 4°, diameter: 3 cm) and a Peltier temperature controller. All the measurements were conducted at a constant temperature of 25 ± 0.2 °C.

2.10. Field-emission scanning electron microscopy (FE-SEM)

A Weiss scanning electron microscope, operated at an accelerating voltage between 0.75 and 2 kV, was used to capture secondary electron images nanofibrillated surface. A drop of the nanofibrillated suspension (with a solid content about 0.2%) was deposited on a surface of silicium wafer and coated with a thin carbon layer applied by sputtering with a thickness being limited to 3–4 nm.

2.11. Dynamic mechanical analysis (DMA)

Dynamic mechanical analysis (DMA) experiments were conducted in tension mode using a PYRIS™ Diamond DMA (Perkin-Elmer, Waltham, MA, USA). Temperature scans were run from −50 °C to 100 °C at a heating rate of 2 °C/min, a frequency of 1 Hz and amplitude of 10 μm. The storage (E') and the loss (E'') *moduli*, as well as the loss factor, $\tan\delta = (E''/E')$, were measured as a function of temperature. Sample dimensions were about 20 mm (length), 10 mm (width) and 0.3–0.5 mm (thickness).

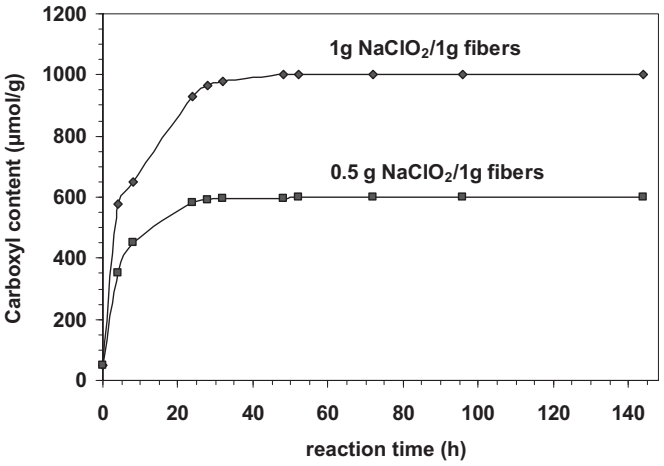

Fig. 1. Carboxyl contents in Eucalyptus cellulose fibres oxidized by TEMPO/NaClO/$NaClO_2$ pH 7: (temperature = 70 °C, TEMPO = 0.01 g/g).

3. Results and discussion

3.1. TEMPO-mediated oxidation of eucalyptus fibres

The TEMPO-mediated oxidation under neutral conditions using $NaClO_2$ as oxidant instead of NaClO was adopted, in order to ovoid significant decrease in polymerization degree of cellulose consecutive to the cleavage of glycoside bonds and to favour the selective oxidation process of the C6 primary hydroxyl groups to carboxyl without leaving residual aldehyde groups (Saito & Isogai, 2004; Shibata & Isogai, 2003).

The typical kinetic plots of TEMPO-mediated oxidation of eucalyptus fibres (Fig. 1) showed a rapid rise in the carboxyl content during the first 10 h, followed by a slight increase up to 24 h leveling off at a plateau, the magnitude of which was determined by the amount of $NaClO_2$ added. For a carboxyl content of about 300, 500 and 1000 μmol/g, the amount of $NaClO_2$ per g of fibres was 0.3, 0.5 and 1 g, respectively, corresponding to 0.5, 0.85 and 1.7 mol of $NaClO_2$ per equivalent anhydro glucosic unit (AGU). Further increase in the $NaClO_2$ amount over 1.7 mol/AGU did not bring about significant rise in the extent of oxidation degree. This is quite expected if we consider that only hydroxyl groups at the C6 position in the non-crystalline region and/or on crystal surfaces of cellulose are accessible to oxidation while the C6 primary hydroxyls inside the cellulose crystallites remain inaccessible. This is in agreement with previous reported work (Montanari, Roumani, Heux, & Vignon, 2005; Saito, Shibata, Isogai, Suguri, & Sumikawa, 2005).

The analyses of the fibres size at the different oxidation levels (Table 1) revealed that the adopted oxidation procedure did not impart detectable breakage of the fibres. Neither the fibres length nor their diameter changed after the TEMPO-mediated oxidation at pH 7 in the presence of $NaClO_2$ as an oxidizing agent.

3.2. Fibrillation of oxidized eucalyptus fibres

Taking into consideration the instant of the appearance of a strong gel during the homogenization process, as the event corresponding to the occurrence of defibrillation giving rise to NFC, then it can be seen from Table 1 that TEMPO-mediated oxidation of the fibres facilitates the defibrillation process and reduces the number of passes necessary to get the gel. However, the significant drop in the number of passes was observed when we went from the virgin pulp up to a carboxyl content of about 300 μmol/g, above which the necessary number of passes remained around 5 passes. Furthermore, it is worth noting that the oxidation treatment the fibrillation

Table 1
Morphological characteristic of the different fibres used and the corresponding number of passes necessary to get the gel.

	Eucal-0	Eucal-200	Eucal-300	Eucal-500	Eucal-1000
Carboxylic content (μmol/g)	80	200 ± 10	300 ± 10	500 ± 20	1000 ± 20
Mean fibre length (μm)	615	625	618	625	645
Mean fibre diameter (μm)	18	19	18	18	19
Number of passes at 300 bar	30**	20*	6*	5*	4*
Yield %					
Initial gel at 300 bar (IG)		30*	40*	72*	77*
IG + 5P600 bar			70	92	92
IG + 10P600 bar			73	95	94
IG + 15P600 bar			85	95	95

* Pressure being maintained constant at 300 bar.
** Multiple clogging.

process easier as it prevents the clogging and obstruction of the homogenizer occurring in the presence of the non-oxidized fibres. The easier fibrillation of TEMPO-mediated oxidized bleached cellulose fibres was probably the result of the combination of different effects; (i) the carboxyl groups generate negative charges that bring forth repulsive forces between microfbrils (Saito et al., 2006) within the cell wall contributing to loosen the microfibrils cohesion held by hydrogen bonding, (ii) the oxidation favours the hydration and the swelling of the fibres making them more flexible and the crystalline zone more accessible. This was noted by Dang et al. pointing an enhancement in the water retention value (WRV) of fibres after TEMPO-mediated oxidation of soft-wood bleached kraft pulp Zheng, Jianguo and Ragauskas (2007), (iii) the oxidation loosens the primary S1 cell wall making the S2 layer more accessible and more prone to fibrillation during the homogenization process, and (iv) the oxidation results in chain scission in the amorphous zone creating weak points within the fibre cell wall facilitating the mechanical fibrillation. However, based on the above analysis, one can rule out any effect in relation to the evolution of the fibre's morphology.

The prominent role of the negative charges in the disintegration process is confirmed by the evolution in the number of passes according to the pH of the pulp suspension. Indeed, for Eucl-500, as the pH of the fibres suspension reached 4 (pH where the major fraction of the carboxyl groups are non ionized), it was observed that the number of passes required to obtain the gel increased up to 30 passes at 300 bar, which is quite similar to one necessary for the non-oxidized eucalyptus fibres to be fibrillated. On the other hand the number of passes remained unchanged (5 passes) as the fibrillation is carried at pH 9. Furthermore, when we reduce the pH of the NFC by the addition of HCl solution, we notice an abrupt formation of coagulum lump when the pH falls down 4. It is obvious that the resulting loss of colloidal stability of the nanofibrillated suspension is the consequence of the protonation of the $-COO^-$ into –COOH, rendering not viable the repulsion among nanofibres to take place. This phenomenon emphasis on the key role of the carboxyl groups in enhancing the colloidal stability of the NFC suspension through electrostatic effects.

From Table 1 and Fig. 2, it can be seen that the magnitude of the pressure during the homogenisation process notably affects the fraction of the non-fibrillated material. Actually, increasing the pressure from 300 to 600 bar reduces the non-fibrillated fraction from 60% to 30% and from 28% to 8% for Eucal-300 and Eucal-500, respectively. Once more, the carboxyl content governs the extent of the defibrillation degree at high pressure. However, over about 500 μmol/g, further growth in the carboxyl content did not bring a further increase in the yield of NFC. Furthermore, over this carboxyl content and at this pressure level, i.e. 600 bar, five additional passes is enough to bring about nearly complete nanofibrillation action. Indeed, the yield in NFC grow to 92% at both a carboxyl content of 500 and 1000 μmol/g after five additional passes at 600 bar, and reached 95% after 10 and 15 additional passes at 600 bar.

The appearance of the ensuing nanofibrillated gel (at 1% solid content and without any dilution) issuing from the oxidized eucalyptus samples following the different stages of the homogenization process, is shown in Fig. 3. For all the samples a translucent gel, whose transparency degree differs according to the carboxyl content, the number of passes and the defibrillation pressure, is obtained. After several passes (4–7) at 300 bar, the fairly higher transparency degree is observed for the highest oxidation degree (Eucal-1000). Conversely, a significant improvement in the transparency is observed after additional passes at 600 bar, namely for the samples with carboxyl content 500 and 1000 μmol/g. To further evidence the effect of the homogenization condition on the transparency of the NFC suspension, the transmittance spectra of a diluted suspension in the range of 400–800 nm was recorded (Fig. 4). As shown in Fig. 4a, for the samples homogenized at 300 bar, the transmittance spectra is shifted towards higher values as the carboxyl content goes up. However, the transmittance remained lower than 60% which is likely to be a consequence of the presence of the non-fibrillated material responsible of the light-scattering phenomenon. A huge increase in transmittance is achieved after 5–10 additional passes at 600 bar, with the most pronounced effect for Eucal-1000 being higher than 90% at 600 nm, as shown in Fig. 4b. This result accounts for the high transparency degree of NFC prepared from Eucal-100 (Fig. 3). However, in spite of similar amount in non-fibrillated fraction in NFC samples prepared from Eucal-500 and Eucal-1000, the higher transparency degree is observed for the later gel, meaning that NFC bearing the higher amount of carboxylic

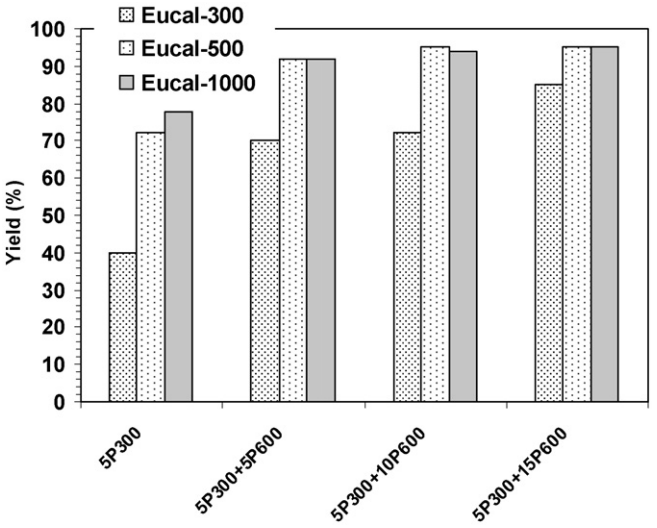

Fig. 2. Yield of nanofibrillated fibres according to the carboxyl content, the number of passes and the fibrillation pressure: (5P300 + 5P600 means, 5 passes at 300 bar followed by 5 passes at 600 bar).

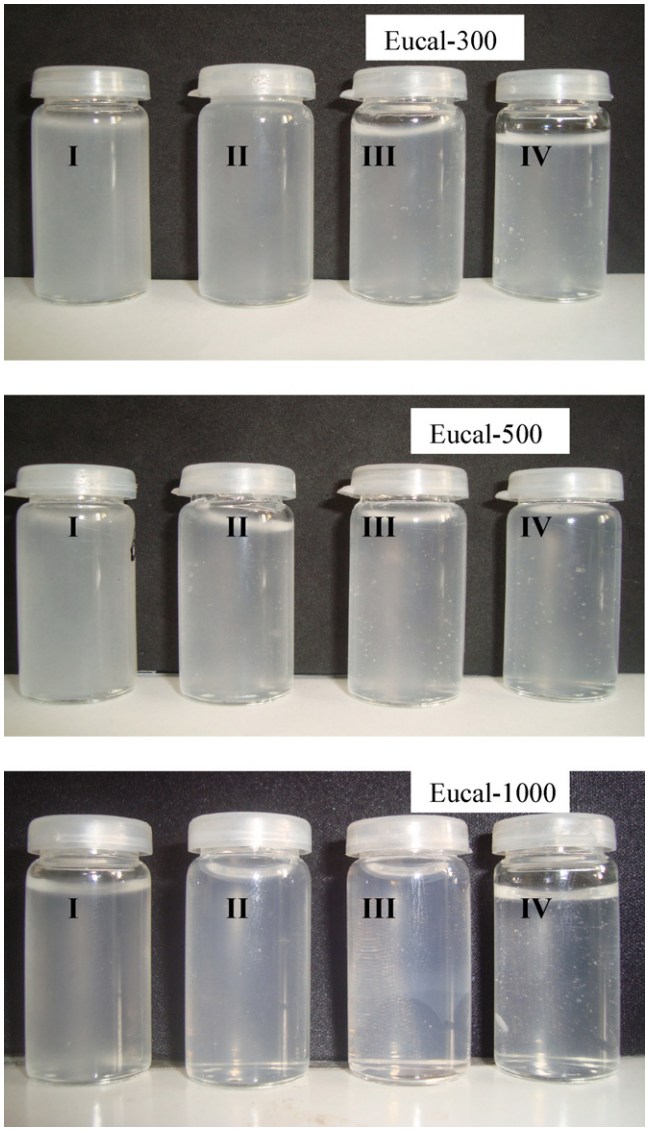

Fig. 3. Appearance of the NFC gel at 1 wt.% issuing from Eucal-300, Eucal-500 and Eucal-100; (I) original gel after several passes at 300 bar, (II) 5 additional passes at 600 bar, (III) 10 additional passes at 600 bar, and (IV) 15 additional passes at 600 bar.

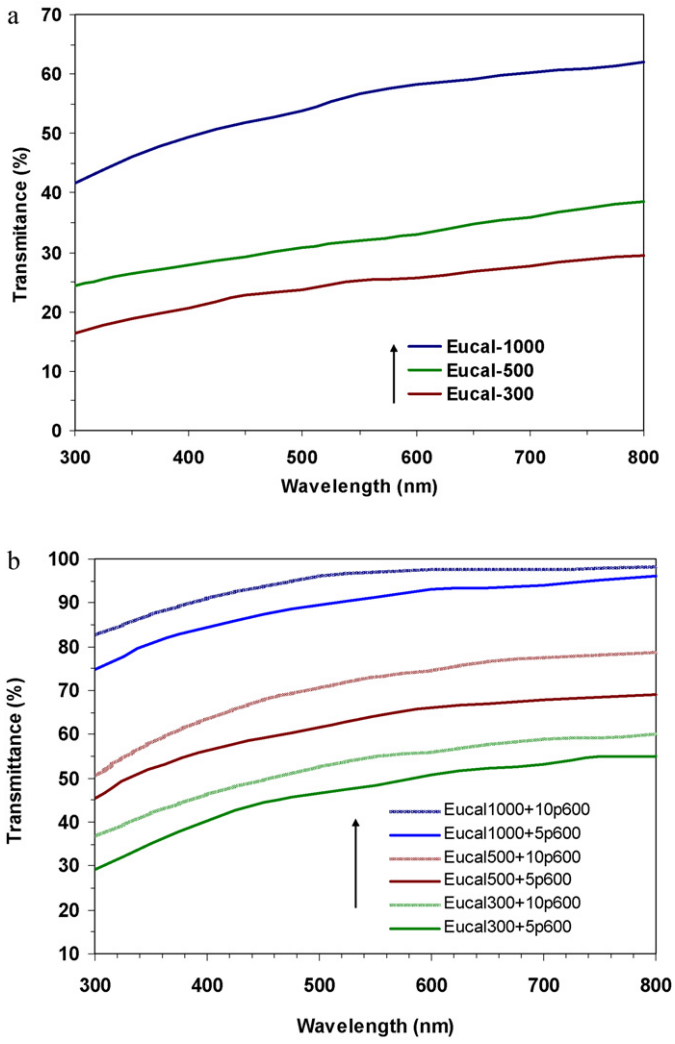

Fig. 4. UV–vis transmittance spectra of the NFC suspension (without any centrifugation) from TEMPO-oxidized eucalyptus fibres; (a) after 5–6 passes at 300 bar, and (b) after additional passes at 600 bar. (Concentration 0.1 wt.% with a 1 cm path length.)

groups exhibits the highest transparency. This phenomenon may arise from their higher dispersion state of the nanofibers. Actually, the ionized carboxylic groups impart electrostatic stabilization as a result of the electrostatic repulsion between the negative charges on the surface of the nanofibres. Thus, the higher the surface charge of the NFC, the less likely is the possibility of interaction or aggregation among nanofibres suspension.

3.3. Morphology of the ensuing NFC

In order to get a more accurate idea about the dimension scale of the prepared nanofibrillated, FE-SEM observation was carried on. Many preliminary trials were necessary before the conditions for the direct observation of the nanofibrillated could be ensured with enough resolution. For this purpose, some conditions were adopted. First, a drop of the NFC suspension (with a solid content about 0.5–0.2%) was deposited on the surface of silicon wafer, able of ensuring electron conduction during the analysis. Next, in order to provide surface electrical conductivity, the sample was coated with a thin carbon layer applied by sputtering with a thickness being limited to 3–4 nm. Finally, the accelerating voltage was maintained at a relatively low range (0.5–1 kV) to ensure good image resolution without any damage to the nanofibers during the analysis.

The observation of the supernatant fraction (Fig. 5) revealed nano-sized fibrils with a width being within the range of 5–20 nm. The distribution of the width is fairly narrow without any trace of visible fragment of fibres. Though the image observed stems from a small drop of a diluted nanofibrillated suspension (0.2%), a thin web-like form of highly interwoven microfibrils overlapping each other is observed for all the samples. This picture provides evidence of the high potential of the cellulose nano-sized fibrils to build up an entangled network through hydrogen bonding when incorporated within polymer matrix. This interwoven structure makes it difficult to estimate the NFC length. Further fibrillation at a higher pressure seems not to affect the width of the fibrils on the supernatant fraction, which is an indication that the nano-sized fibrils on the supernatant fraction correspond really to the ultimate nanofibrils building up the fibres.

The sediment fraction was formed by macroscopic fibres with a width varying between 2 and 20 μm and a length exceeding 500 μm. A higher magnification of the fibre's surface showed a bundle of fibril aggregates similar in their aspect to the one observed on the supernatant fraction. This provides evidence that the ensuing nanofibrillated resulted from the physical break-up of the aggre-

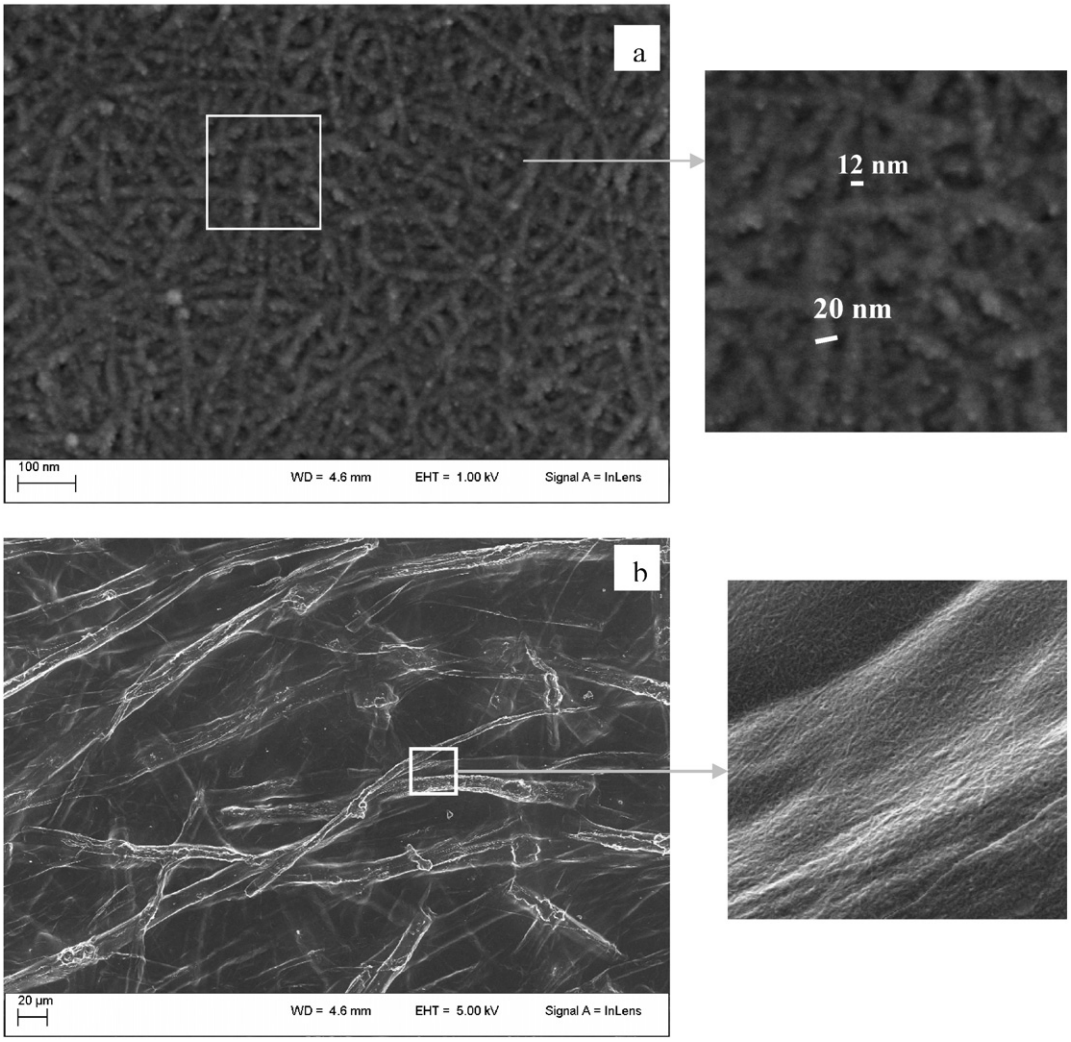

Fig. 5. FE-SEM pictures of (a) the supernatant fraction of high-pressure homogenized fibres from Eucal-500, after 5 passes at 300 bar, and (b) the sediment fraction.

gated microfibrils within the cell wall of the fibres without any degradation effect.

3.4. Rheological behaviour of nanofibrillated

The shear rate dependence of the viscosity for the 1.5 wt.% nanofibrillated suspension with different oxidation extent, shown in Fig. 6, reveals two Newtonian plateau, one at a low shear rate, and the other at a high shear rate, separated by a shear thinning behaviour. This behaviour is also a characteristic of cellulose whiskers dispersion (Ebeling et al., 1999) and microcrystalline cellulose hydrogels (Ono et al., 1998). The high viscosity at a low shear rate can be related to the morphology of NFC with a length exceeding several μm and a nano-sized diameter. This leads to the entanglement and connection of the fibrils giving rise to a strong network structure held through hydrogen bonding. Such network accounts for the gel character of the NFC dispersion on the first Newtonian plateau. Beyond a critical shear rate, the shear forces are enough to overcome the hydrogen interaction holding the NFC network, leading to a progressive breakdown of the network which account for the shear thinning behaviour.

The change in the carboxyl content of the nanofibrillated gel does not bring a significant change in the rheological behaviour with the carboxyl content up to 500 μmol/g (NFC from Eucal-300 and Eucal-500). On the other hand, a lower viscosity is observed for the NFC sample with the highest carboxyl content (Eucal-1000), although the samples presented the highest yield of fibrillation. It is likely that the electrostatic repulsion resulting from the presence of a high level of ionized carboxyl groups on the surface of the nanofibres reduces the extent of the interaction among NFC resulting in a lower viscosity of the suspension. This effect accounts equally for the higher transmittance and transparency of the NFC from Eucal-1000, as reported above.

The number of passes, at a high pressure (600 bar), affects also the rheological behaviour, bringing about an increase in the gel viscosity as shown in Fig. 6. This effect is probably due to a higher fibrillation action promoted by the multiplication of the number of passes at a high pressure leading to a higher yield in nanofibrillated fraction and a stronger network structure.

3.5. Crystallinity change of NFC

The normalized XRD patterns of the original eucalyptus fibres and that of the different samples of NFC prepared at a different number of passes are shown in Fig. 7. The original eucalyptus fibres exihibit a sharp high peak at $2\theta = 22.6^{\circ}$, which is assigned to the [0 0 2] lattice plane of cellulose I. The two overlapped weaker diffractions at 2θ close to 14.8 and 16.3 are assigned to the [1 0 1] and [$10\bar{1}$] lattice planes of cellulose I (Heritage, Mann, & Roldan-Gonzalez, 1963).

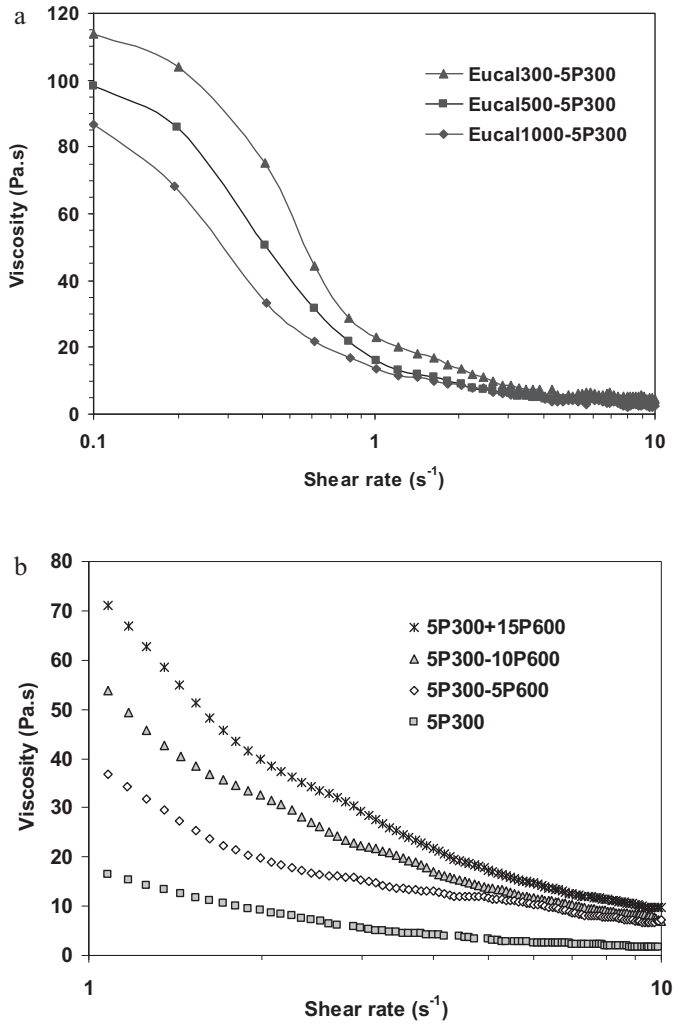

Fig. 6. Viscosity as a function of shear rate of the NFC gel at 1.5 wt.% solid content (a) obtained after 5–6 passes at 300 bar according to the carboxyl content, and (b) for NFC from Eucal-1000 after additional passes at 600 bar. (5p300–5p600: meaning 5 passes at 300 bar + 5 passes at 600 bar). Measurement temperature: 25 °C.

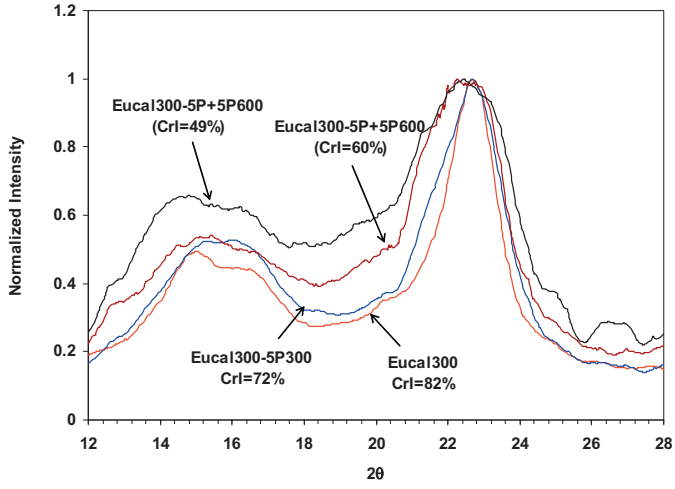

Fig. 7. X-ray diffractogram patterns of the original oxidized fibres and the corresponding NFC after different passes at 300 and 600 bar: (Eucal-300: oxidized eucalyptus fibres with a carboxyl content 300 μmol/g; Eucal-300–5P300: Eucal-300 after 5 passes at 300 bar; Eucal-300–5P600: Eucal-300–5P300 after 5 additional passes at 600 bar).

The CrI of the different nanofibrillated samples, original and oxidized fibres was calculated on the basis of X-ray analysis using Eq. (1). Compared with the original fibres, both of the oxidized fibres and of the NFC samples did not exhibit any evolution in their polymorph type. The crystalline degree did not go through any significant evolution upon the oxidation treatment. Such result, in agreement with previous reported work, is the consequence of the restriction of the oxidation to the crystallite surfaces and the disordered regions (Montanari et al., 2005; Saito & Isogai, 2004). However, as shown in Fig. 7 the CrI decreased with the fibrillation action. The higher the number of passes and the fibrillation pressure the more notable the drop in the crystalline degree is. It passes from 82% for the original fibres to 72% after 5 passes at 300 bar and to, 60% and 49% after additional 5, and 10 passes at 600 bar, respectively. It is likely that a high shearing action during the homogenization process may result in damage either through breaking effect or peeling-off of the cellulose chains on the surface of the crystallite. This result disagrees with that of Heux, Dinand and Vignon (1999) and Agoda-Tandjawa et al. (2010) who observed that the fibrillation treatment resulting from multiple passages through two-stages homogenization, did not affect cellulose crystallinity. However, the method used to estimate the crystallinity is based CP-MAS NMR analysis which is less accuracy than DRX measurement.

3.6. DMA analysis of nanocomposite film

To investigate the reinforcement efficiency of the ensuing NFC, nanocomposite films were prepared by mixing NFC suspension with an aqueous dispersion a commercial of poly(S-co-BuA) latex as a matrix. The ensuing films were analysed by DMT. The temperature dependence of the storage tensile modulus E' and loss angle $\tan\delta$ as a function of temperature at 1 Hz for the unfilled matrix with different NFC contents are shown in Fig. 8a.

At low temperature, the storage modulus did undergo only a slight enhancement with respect to the unfilled matrix (not shown here because of the normalization). This is quite expected given the relatively low volume fraction of the reinforcing phase. On the contrary, above the glass transition the storage modulus increased significantly upon NFC addition, as much higher as the NFC loading is going up, which is in line with the well-known reinforcing effect of cellulose nanofibres.

To get more insights on the stiffening effect imparted by the addition of NFC, the evolution of the relative modulus $E_r = (E_{com}/E_{mat})$ (with E_{com} and E_{mat} are the storage modulus of the nanocomposite and unfilled matrix, respectively, measured at 60 °C, i.e. around the T_g value +40 °C), vs. the NFC content is shown in (Fig. 8b). The continuous rise in the relative modulus clearly confirmed the strong reinforcing potential of the prepared NFC. As an example, the modulus is 118 times higher than that of the unfilled matrix after the addition of 4 wt.%. This result is in agreement with other reported work using NFC from other origin (Bendahou et al., 2010; Malainine et al., 2005a). Conversely, one can clearly note a change in the slope of the curve being steeper over 2 wt.% content, which indicates a more reinforcing potential of the NFC over this threshold. This high reinforcing effect above a critical level, is common to cellulose based nanofiller, and is attributed to the formation of a stiff percolating network held by strong hydrogen bonds between adjacent nanofibres (Azizi Samir et al., 2004). The percolation threshold (ϕ_p) can be determined by applying a power law function to the E' vs. whiskers loading according to the following equation:

$$E' \propto (\phi - \phi_p)^n \text{ for } \phi > \phi_c$$

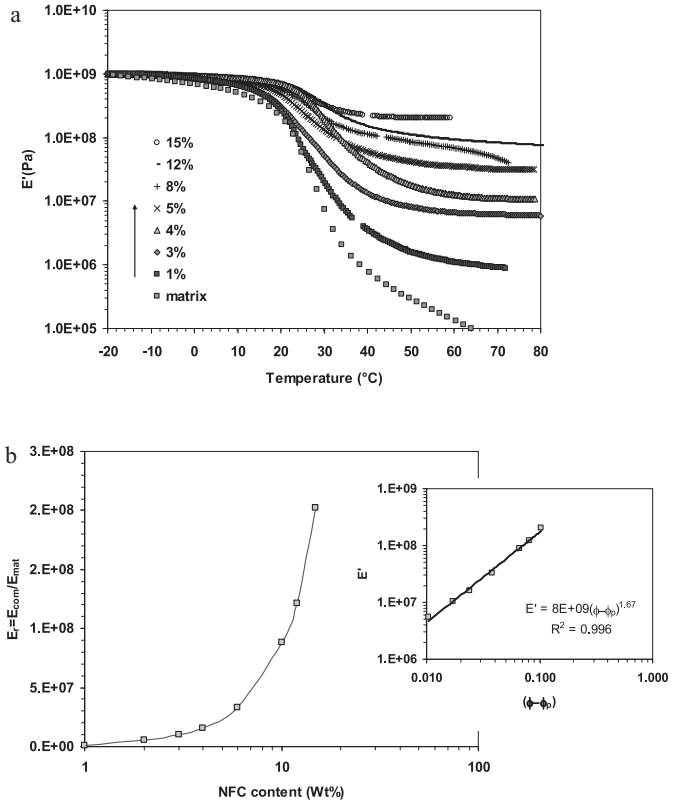

Fig. 8. Evolution of the (a) storage tensile modulus E' vs. temperature at 1 Hz, and (b) storage tensile modulus vs. NFC content at 60 °C, for nanocomposite film prepared from Eucal-500 gel and acrylic latex. (The inset represents E' vs. $(\phi - \phi_p)$, where ϕ and ϕ_p represents the volume fraction of the reinforcement and the percolation threshold).

The linear fit for E' vs. $(\phi - \phi_p)$ on a log–log scale was found for the percolation threshold ϕ_p being close to 0.3 vol% and critical exponent t equal to 1.7 (see inset in Fig. 8b).

For all the nanocomposites as well as the neat matrix, the tan δ trace exhibits a well-defined relaxation (α relaxation) around 26 °C associated with the cooperative motions of long chain sequences. The addition of NFC resulted in the following trend: (i) a continuous drop of its magnitude, (ii) a shift towards lower temperatures which is a consequence of a coupling effect, and (iii) a broadening in the tan δ peak attested by the increase in the line-width at half-maximum height. These two effects are often observed in cross-linked polymers (Ward & Sweeney, 2004) and are indicative of reduced polymer chain mobility resulting from the nanofibers acting as physical entanglements

4. Conclusion

The effect of the TEMPO-mediated oxidation treatment of eucalyptus pulp on facilitating the defibrillation process under high pressure was investigated in the present work. NFC was prepared using homogenization under pressure ranging from 300 up to 600 bar. What can be concluded from the present study is that:

1. The TEMPO-mediated oxidation treatment facilitates the defibrillation process, reduces the number of passes necessary to get the gel and prevents clogging of the homogenizer.
2. A carboxyl content about 300 μmol/g is necessary to significantly reduce the number of passes down to 7–5 passes, to obtain the gel.
3. Over a carboxyl content of about 500 μmol/g, the yield in the NFC exceeds 90%, after 5 passes at 600 bar.
4. FE-SEM confirms the nanosized scale of NFC with width being in the range of 5–20 nm.
5. The highest transparency degree is attained when the carboxyl content exceeds 500 μmol/g and under a fibrillation pressure about 600 bar.
6. The incorporation of the ensuing NFC to a polymer matrix imparts a high reinforcing effect confirmed by the huge enhancement in the tensile modulus. As an example, the modulus was multiplied by a factor 118 with respect to unfilled matrix upon incorporation of 4 wt.% NFC.

References

Abe, K., Iwamoto, S., & Yano, H. (2007). Obtaining cellulose nanofibers with a uniform width of 15 nm from wood. *Biomacromolecules*, *9*(3), 1022–1026.

Agoda-Tandjawa, G., Durand, S., Berot, S., Blassel, C., Gaillard, C., Garnier, C., et al. (2010). Rheological characterization of microfibrillated cellulose suspensions after freezing. *Carbohydrate Polymers*, *80*, 677–686.

Alemdar, A., & Sain, M. (2008). Isolation and characterization of nanofibers from agricultural residues–Wheat straw and soy hulls. *Bioresource Technology*, *99*, 1664–1671.

Azizi Samir, M. A. S., Alloin, F., Paillet, M., & Dufresne, A. (2004). Tangling effect in fibrillated cellulose reinforced nanocomposites. *Macromolecules*, *37*, 4313–4316.

Bendahou, A., Kaddami, H., & Dufresne, A. (2010). Investigation on the effect of cellulosic nanoparticles morphology on the properties of natural rubber based nanocomposites. *European Polymer Journal*, *46*, 609–620.

Bledzki, A. K., & Gassan, J. (1999). Composites reinforced with cellulose based fibres. *Progress in Polymer Science*, *24*, 221–274.

Boldizar, A., Klason, C., Kubat, J., Naslund, P., & Saha, P. (1987). Prehydrolyzed cellulose as reinforcing filler for thermoplastics. *International Journal of Polymer Materials*, *11*(4), 229–262.

Ebeling, T., Paillet, M., Borsali, R., Diat, O., Dufresne, A., Cavaille, Y., et al. (1999). Shear-induced orientation phenomena in suspensions of cellulose microcrystals. Revealed by small angle X-ray scattering. *Langmuir*, *15*(19), 6123–6126.

Henriksson, M., Henriksson, G., Berglund, L. A., & Lindstrom, T. (2007). An environmentally friendly method for enzyme-assisted preparation of microfibrillated cellulose (nanofibrillated) nanofibers. *European Polymer Journal*, *43*, 3434–3441.

Heritage, K. J., Mann, J., & Roldan-Gonzalez, L. (1963). Crystallinity and the structure of celluloses. *Journal of Applied Polymer Science*, *1*, 671–685.

Herrick, F. W., Casebier, R. L., Hamilton, J. K., & Sandberg, K. R. (1983). Microfibrillated cellulose: Morphology and accessibility. *Journal of Applied Polymer Science: Applied Polymer Symposium*, *37*, 797–813.

Heux, L., Dinand, E., & Vignon, M. R. (1999). Structural aspects in ultrathin cellulose microfibrils followed by C-13 CP-MAS NMR. *Carbohydrate Polymers*, *40*(2), 115–124.

Iwamoto, S., Abe, K., & Yano, H. (2008). The effect of hemicelluloses on wood pulp nanofibrillation and nanofiber network characteristics. *Biomacromolecules*, *9*(3), 1022–1026.

Iwamoto, S., Nakagaito, A. N., Yano, H., & Nogi, M. (2005). Optically transparent composites reinforced with plant fiber-based nanofibers. *Applied Physics A*, *81*, 1109–1112.

Jacob, M. J., & Thomas, S. (2008). Biofibres and biocomposites. *Carbohydrate Polymers*, *71*, 343–364.

Johnson, R. K., Zink-Sharp, A., Renneckar, S. H., & Glasser, G. W. (2009). A new bio-based nanocomposite: Fibrillated TEMPO-oxidized celluloses in hydroxypropylcellulose matrix. *Cellulose*, *16*, 227–238.

Leitner, J., Hinterstoisser, B., Wastyn, M., Keckes, J., & Gindl, W. (2007). Sugar beet cellulose nanofibril-reinforced composites. *Cellulose*, *14*, 419–425.

Malainine, M. E., Mahrouz, M., & Dufresne, A. (2005a). Thermoplastic nanocomposites based on cellulose microfibrils from Opuntia ficus-indica parenchyma cell. *Composite Science Technologies*, *65*, 1520–1526.

Malainine, M. E., Mahrouz, M., & Dufresne, A. (2005b). Thermoplastic nanocomposites based on cellulose microfibrils from, Opuntia ficus-indica parenchyma cell. *Composite Science Technology*, *65*, 1520–1526.

Mohanty, A. K., Misra, M., & Drzal, L. T. (2001). Surface modifications of natural fibers and performance of the resulting biocomposites: An overview. *Computer Interfaces*, *8*, 313–343.

Montanari, S., Roumani, M., Heux, L., & Vignon, M. R. (2005). Topochemistry of carboxylated cellulose nanocrystals resulting from TEMPO-mediated oxidation. *Macromolecules*, *38*, 1665–1671.

Nakagaito, A. N., & Yano, H. (2004). The effect of morphological changes from pulp fiber towards nano-scale fibrillated cellulose on the mechanical properties of high-strength plant fiber based composites. *Material Science and Processing*, *78*, 547–552.

Nishino, T., Takano, K., & Nakamae, K. (1995). Elastic-modulus of the crystalline regions of cellulose polymorphs. *Journal of Polymer Science, Part B: Polymer Physics*, *33*, 1647–1651.

Ono, H., Yamada, H., Matsuda, S., Okajima, K., Kawamoto, T., & Iijima, H. (1998). ^{1}H NMR relaxation of water molecules in the aqueous microcrystalline cellulose suspension systems and their viscosity. *Cellulose*, *5*(4), 231–247.

Pääkkö, M., Ankerfors, M., Kosonen, H., Nykanen, A., Ahola, S., Osterberg, M., et al. (2007). Enzymatic hydrolysis combined with mechanical shearing and

high-pressure homogenization for nanoscale cellulose fibrils and strong gels. *Biomacromolecules*, *8*, 1934–1941.

Saito, T., Hirota, M., Tamura, N., Kimura, S., Fukuzumi, H., Heux, L., et al. (2009). Individualization of nano-sized plant cellulose fibrils by direct surface carboxylation using TEMPO catalyst under neutral conditions. *Biomacromolecules*, *10*, 1992–1996.

Saito, T., & Isogai, A. (2004). TEMPO-mediated oxidation of native cellulose. The effect of oxidation conditions on chemical and crystal structures of the water-insoluble fractions. *Biomacromolecules*, *5*, 1983–1989.

Saito, T., Kimura, S., Nishiyama, Y., & Isogai, A. (2007). Cellulose nanofibers prepared by TEMPO-mediated oxidation of native cellulose. *Biomacromolecules*, *8*, 2485–2491.

Saito, T., Nishiyama, Y., Putaux, J. L., Vignon, M., & Isogai, A. (2006). Homogeneous suspensions of individualized microfibrils from TEMPO-catalyzed oxidation of native cellulose. *Biomacromolecules*, *7*, 1687–1691.

Saito, T., Shibata, I., Isogai, A., Suguri, N., & Sumikawa, N. (2005). Distribution of carboxylate groups introduced into cotton linters by the TEMPO-mediated oxidation. *Carbohydrate Polymers*, *61*, 414–419.

Segal, L., Creely, J. J., Martin, A. E., & Conrad, C. M. (1959). An empirical method for estimating the degree of crystallinity of native cellulose using the X-ray diffractometer. *Textile Research Journal*, *29*, 786–794.

Shibata, I., & Isogai, A. (2003). Depolymerization of cellouronic acid during TEMPO-mediated oxidation. *Cellulose*, *10*, 151–158.

Siro, I., & Plackett, D. (2010). Microfibrillated cellulose and new nanocomposite materials: A review. *Cellulose*, *17*(3), 459–494.

Turbak, A. F., Snyder, F. W., & Sandberg, K. R. (1983). Microfibrillated cellulose, a new cellulose product: Properties, uses, and commercial potential. *Journal of Applied Polymer Science: Applied Polymer Symposium*, *37*, 815.

Wågberg, L, Decher, G., Norgren, M., Lindström, T., Ankerfors, M., & Axnäs, K. (2008). The build-up of polyelectrolyte multilayers of microfibrillated cellulose and cationic polyelectrolytes. *Langmuir*, *24*(3), 784–795.

Ward, I. M., & Sweeney, J. (2004). *An introduction to the mechanical properties of solid polymers* (2nd ed.). J. Wiley & Sons Ltd.

Zheng, D., Jianguo, Z., & Ragauskas, A. J. (2007). Characterizing TEMPO-mediated oxidation of ECF bleached softwood Kraft pulps. *Carbohydrate Polymers*, *70*, 310–317.